Comptes Rendus

Physique

Yao Pei, Lionel Pichon, Mohamed Bensetti and Yann Le Bihan

Analysis of inductive power transfer systems by metamodeling techniques

Research article / *Article de recherche*

Energy in the heart of EM waves: modelling, measurements and management / *L'énergie au cœur des ondes électromagnétiques : modélisation, mesures et gestion*

Analysis of inductive power transfer systems by metamodeling techniques

Analyse de systèmes de transfert de puissance inductifs par des techniques de métamodélisation

Yao Pei [*, a, b], **Lionel Pichon** [a, b], **Mohamed Bensetti** [a, b] **and Yann Le Bihan** [a, b]

[a] Université Paris-Saclay, CentraleSupélec, CNRS, Laboratoire de Génie Electrique et Electronique de Paris, 91192, Gif-sur-Yvette, France

[b] Sorbonne Université, CNRS, Laboratoire de Génie Electrique et Electronique de Paris, 75252, Paris, France

E-mail: yao.pei@centralesupelec.fr (Y. Pei)

Abstract. This paper presents some metamodeling techniques to analyze the variability of the performances of an inductive power transfer (IPT) system, considering the sources of uncertainty (misalignment between the coils, the variation in air gap, and the rotation on the receiver). For IPT systems, one of the key issues is transmission efficiency, which is greatly influenced by many sources of uncertainty. So, it is meaningful to find a metamodeling technique to quickly evaluate the system's performances. According to the comparison of Support Vector Regression, Multigene Genetic Programming Algorithm, and sparse Polynomial Chaos Expansions (PCE), sparse PCE is recommended for the analysis due to the tradeoff between the computational time and the accuracy of the metamodel.

Résumé. Ce papier présente différentes techniques de métamodélisation afin d'analyser la variabilité des performances d'un système de transfert de puissance par induction (IPT), en tenant compte des sources d'incertitude (décentrage des bobines, la variation de l'entrefer et la rotation du récepteur). Pour les systèmes IPT, l'une des questions clés est l'efficacité de la transmission, qui est fortement influencée par les nombreuses sources d'incertitude. Il est donc important de déterminer une technique de métamodélisation susceptible d'évaluer rapidement les performances du système. Trois techniques de métamodélisation sont comparées : la régression à vecteurs de support, l'algorithme de programmation génétique multigénique et les développements du chaos polynomial (PCE), il ressort que la technique PCE est recommandée pour une telle analyse en raison du compromis entre le temps de calcul et la précision du métamodèle.

*Corresponding author

1. Introduction

Around 800 million vehicles with internal combustion engines (ICEs) are used worldwide [1]. These vehicles are a major source of greenhouse gases, especially CO_2. Thus, a practical way of dealing with the global warming problem is to replace ICE-powered vehicles with electric vehicles (EVs) [1–3]. The use of electric cars also improves the quality of air around major cities. To replace ICEs, many vehicle companies are developing "plug-in" EVs, which use lithium-ion (or polymer) batteries that can be recharged at home or at charging stations [2,3]. But the promotion and adoption of plug-in EVs raise many questions. First, the cost of lithium batteries is high. Second, the batteries are heavy. Third, to decrease the charging time for the battery, it requires an expensive infrastructure for charging stations [2–7]. Finally, mishandling the high-power cables will lead to security problems [3, 4, 8, 9]. So, due to these problems, inductive power transfer (IPT) has been introduced as an alternative technology, allowing power flow in a contactless manner. Using a resonant IPT system seems to be an effective technology for the growth of the EVs market [10]. Moreover, its application for the charge during the vehicle's motion is promising to overcome the barriers of heavy onboard battery storage and the long recharging time [3,4,8,9]. IPT is essentially based on the resonance of two magnetically coupled inductors (constituting the coupler): the transmitter, placed on the ground, and the receiver, placed under the vehicle floor.

In a real IPT system scenario, various receiver positions may happen during the park or driving [9]. A careful design process of IPT systems requires considering multiple parameters (misalignment, relative rotation of the receiver, air gap, etc.). So, when using simulation tools, multiple 3D numerical computations are needed to assess the performance of the IPT system when these situations happen. Nevertheless, using complex simulation tools (such as the finite element method) leads to high computational costs for wide parametric analysis. In this case, a standard Monte Carlo (MC) analysis becomes challenging regarding computer resources and simulation time [11, 12].

To solve this problem, "metamodeling techniques" for the parametric and statistical analysis in complex nonlinear problems have been developed. These approaches can reduce the computational cost by substituting an expensive computational model with a so-called metamodel, an analytical approximation of the original model that is much faster to evaluate [11–15]. The metamodels are constructed by learning the varying trend from input parameters and their corresponding model responses, for example, generated from running 3D FEM computations. Because it is faster to evaluate, a metamodel allows more sophisticated analyses, such as sensitivity analysis [16, 17]. In recent literature, several metamodeling techniques have been applied to generate some metamodels trained with a limited set of simulation results, such as Support Vector Regression (SVR) [18], Multigene Genetic Programming Algorithm (MGPA) [19], Polynomial Chaos Expansions (PCE) [20], and so on. Reference [14] focuses on applying the SVR with polynomial kernels to the uncertainty quantification and the parametric modeling of structures. Then, references [14, 15] compare the accuracy and robustness to noise among the SVR, the least squares SVR [21], and the sparse PCE. In the domain of inductive power transfer, a MGPA metamodel is investigated to express the self-inductance and the mutual inductance of the IPT system versus geometrical parameters of the ferrite and coils, so new equations are proposed for evaluating these values of the inductances [22–24]. In [25], sources of uncertainties have been analyzed with different shapes of small-scale couplers by the sparse PCE. Reference [26] has compared the MGPA and sparse PCE metamodeling techniques for the design of IPT systems. Since the design of realistic IPT systems involves complex configurations including many parameters, choosing a fast metamodel is a key point. Comparing different metamodeling techniques in the real-scale couplers for IPT systems is required, and it is important to prove the efficiency in a realistic experiment.
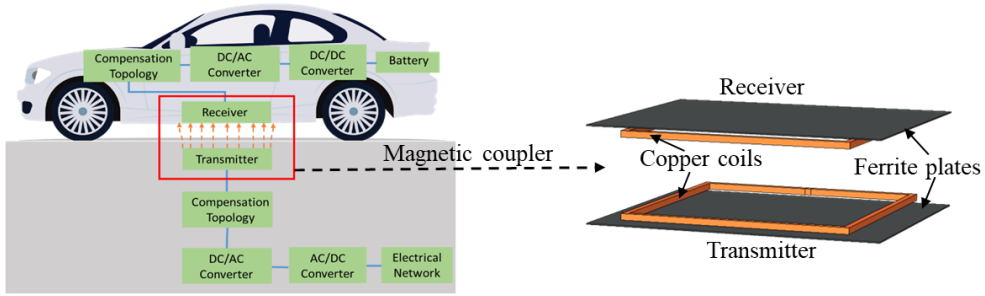
Figure 1. Block diagram of an IPT system.

Therefore, the paper aims to compare several metamodeling techniques for analyzing the mutual inductance of IPT systems, considering the sources of uncertainty (misalignment along the X/Y-axis, variation in air gap, and receiver rotation). First, in Section 2, a 3D model of a practical IPT system is built and numerical predictions related to the electrical parameters and stray magnetic field are validated against experimental measurements. Then, different metamodeling techniques about SVR with the Gaussian radial base function (RBF) kernel, MGPA, and PCE are introduced in Section 3. After, in Section 4, a comparison is presented among these different metamodels for the analysis of square couplers, considering the sources of uncertainty. Finally, the conclusion is given in Section 5.

2. IPT system

2.1. *IPT system introduction*

Figure 1 shows the block diagram of an IPT system for EVs. The system consists of a transmitter, a receiver, converters, and compensation networks for the transmitter and the receiver. The electrical network provides a voltage through the AC/DC converter. The magnetic field produced by the transmitter induces an alternating magnetic field in the receiver. The converters then rectify the AC power to charge the battery. Due to the dimensions of the coils, the parasitic capacitance is insufficient to ensure the resonance in the operational frequency range. Consequently, compensation networks (such as capacitors) are connected to the transmitter and receiver (the self-inductance of the transmitter and the receiver) to adjust the operational frequency and create the resonant state [3, 4, 8, 9, 27–30]. It minimizes the reactive power supply and improves both the transmission efficiency and the power transfer capability.

In the system, the magnetic coupler (indicated in the red line frame) is the key part, which normally includes a pair of coils, ferrite plates, and shielding [3, 4, 8, 9, 27–30]. The geometry and configuration of the coils are crucial for determining the magnetic field of the IPT system and its efficiency. The ferrite plates influence the efficiency and prevent magnetic flux leakage. The shielding is used to prevent magnetic flux leakage, which is usually placed above the receiver to minimize the flux leakage around the system. Some of the IPT systems take the vehicle chassis as conductive material for shielding [31]. For the IPT system transmission efficiency, circuit models with lumped parameters are often used, and the compensation networks are designed to minimize the reactive component of the power supply. Following [3, 4, 8, 9, 27, 29–34], the series–series (SS) compensation network is taken into account to analyze the power transmission efficiency of the system, as shown in Figure 2. Indeed, according to [3, 4, 8, 9, 27, 29–34], it is suitable for the IPT systems, and the condition of resonance in the SS compensation remains
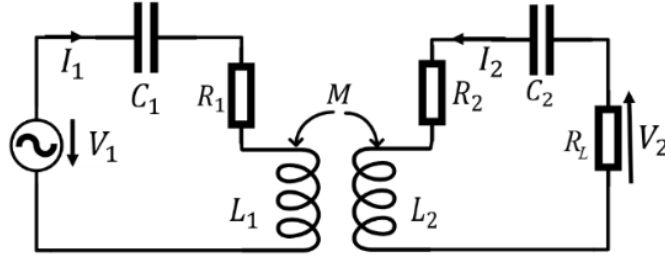
Figure 2. Equivalent electrical circuit in the SS compensation topology [3, 4, 8, 9, 27, 29–34].

Table 1. Parameters of the magnetic coupler

Parameter	Value (Unit)
Exterior length of the coils l_{ex}	468 (mm)
Interior length of the coils l_{in}	442 (mm)
Coil thickness d_c	13 (mm)
Ferrite length l_f	600 (mm)
Ferrite width w_f	500 (mm)
Ferrite thickness t_f	2 (mm)
Distance between the coils and the ferrite	8 (mm)
Ferrite relative permeability μ_r	2000
Cross-sectional area of the wires S	9.82 (mm^2)
Air gap	150 (mm)

constant, independently of the variations of the mutual inductance and the load R_L. L_1 and L_2 represent the self-inductances of the transmitter and the receiver, respectively; R_1 and R_2 represent the resistances of the transmitter and the receiver, respectively; C_1 and C_2 are the resonant capacitors; M is the mutual inductance between the transmitter and the receiver.

So, the equation to calculate the maximum transmission efficiency η_{max} of the system in Figure 2 can be achieved as below when the transmitter and the receiver are identical [32–34]:

$$\eta_{max} \approx 1 - \frac{2}{kQ} = 1 - \frac{2\sqrt{R_1 R_2}}{w_0 M} = 1 - \frac{R_1}{\pi f_0 M} \tag{1}$$

where the coupling coefficient $k = M/\sqrt{L_1 L_2}$; the system quality factor $Q = 2\pi f_0 \sqrt{L_1 L_2 / R_1 R_2}$ [35–37]; f_0 is the resonant frequency.

2.2. *IPT system experimental validation*

In this work, a square coupler was built in the GeePs laboratory, and shown in Figure 3. The square shape is proven in [33, 34] to be well-suited for IPT systems. The parameters of the coupler are summarized in Table 1 [33, 34]. The square coupler has six turns arranged in two layers. These turns are made with litz wires composed of 1250 strands, and the strand's diameter is 0.1 mm, so it is smaller than the skin depth at the operating frequency [34]. The operating frequency of the IPT system is around 85 kHz [33–36, 38].

Then, the magnetic parameters of the square coupler are simulated in COMSOL 6.1 [39] and measured by a RLC meter (Wayne Kerr 4300), and the results are given in Table 2. The relative errors between the measurement and the simulation are around 10%, which may be caused by the real coil shape that is not exactly the same as defined in the simulation. Also,
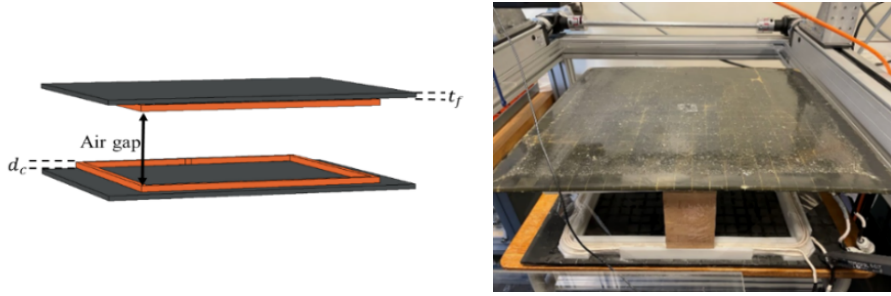
(a) Square magnetic coupler
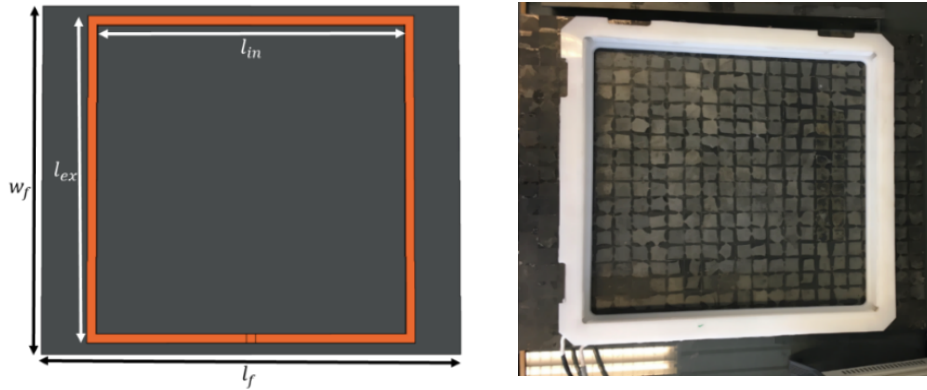
(b) Size of the square magnetic coupler

Figure 3. Simulation model and experimental model of the square magnetic coupler.

**Table 2.** Comparison of the magnetic parameters in the simulation and the measurement

Frequency = 85 (kHz)	Self-inductance L (μH)	Mutual inductance M (μH)	Coupling coefficient k
Simulation	63.7	13.4	0.21
Measurement	58.5	12.1	0.20
Relative error of the experiment (%)	8.1%	9.7%	4.8%

some uncertainty exists about the winding arrangement in the real coil, which may not be well positioned in two layers.

The magnetic flux density distribution is measured at 150 mm above the receiver as shown in Figure 4. The method to do the measurement in the near-field test bench is presented in [34]. The magnetic probe measures the magnetic field and the robot moves the magnetic probe automatically for different measurement positions.

Figure 5 compares the measured and simulated B_{norm} (the norm of the magnetic flux density) on the measurement line as depicted in Figure 4. The relative error between the measured and simulated B_{norm} is around 10%. There exist differences in the position and the amplitude of the magnetic flux density, probably because the coils of the coupler are made by hand. Hence, they are not exactly the same as those defined in the simulation. Moreover, the ferrite plate in the experiment is not as flat as it is in the simulation. Consequently, the magnetic flux density values of the measurement line are not the same as those in the simulation.
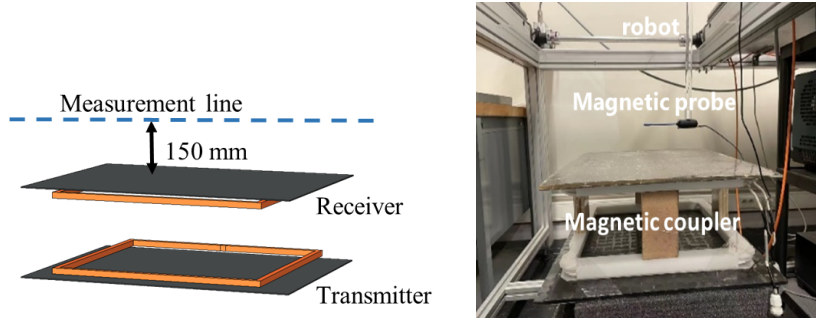
Figure 4. Measurement line of the magnetic flux density above the receiver.
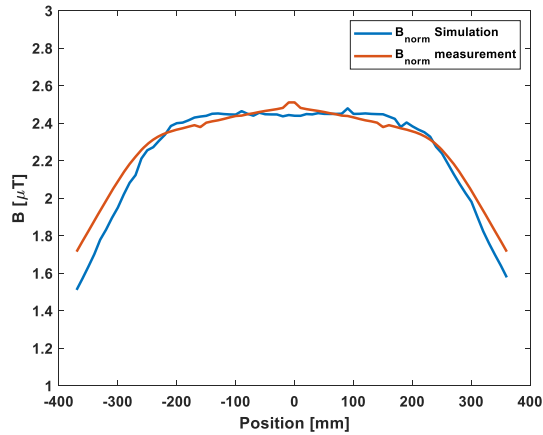
Figure 5. Comparison of the magnetic flux density B_{norm} obtained by the simulation and measurement.

From the results presented above, the reliability of the 3D coupler model has been confirmed through the comparison between the simulated values and the measurement values both for the mutual inductance and the magnetic flux density.

2.3. *Uncertain parameters in the IPT System*

To investigate the efficiency of the IPT system, it is mandatory to consider the sources of uncertainty, such as variations in the misalignment of the receiver due to imperfect parking alignment and variations in the air gap due to loading or unloading the vehicle. Figure 6 shows the rotation angle along the Z-axis α, the misalignment along the X-axis Δx, the misalignment along the Y-axis Δy, and the air gap between two coils Δz for the couplers.

Before performing the uncertainty analysis, it is necessary to assume a probability distribution for the sources of uncertainty. Here, a Gaussian distribution is chosen for these influencing factors, which conforms to the probability that may happen in reality. The statistical parameters of the influencing factors are displayed in Table 3. The range of the air gap and the rotation angle along the Z-axis are referred to [38]. Meanwhile, the range for the misalignment along the X/Y-axis is considered reasonable due to the size of the parking space and the size of the EV chassis.

A parametric sweep for all these influencing factors is very time-consuming. So, it is relevant to build a metamodel using the COMSOl simulation results, which will help save computational
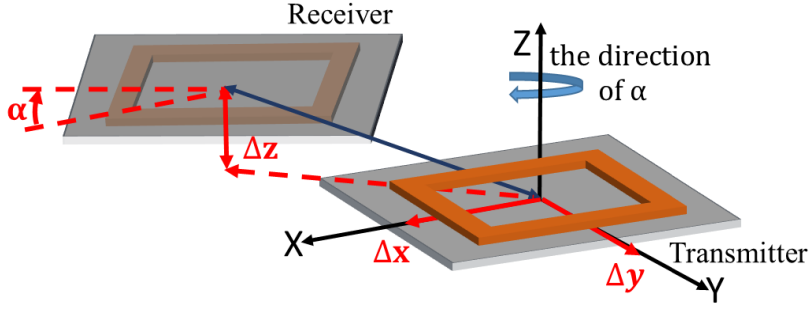
Figure 6. Influencing factors for the square couplers.

Table 3. Properties of the influencing factors

Parameters	Symbol	Distribution	Mean value	Standard deviation
Misalignment along X-axis (mm)	Δx	Gaussian	0	150
Misalignment along Y-axis (mm)	Δy	Gaussian	0	150
Air gap between two coils (mm)	Δz	Gaussian	150	20
Rotation angle along Z-axis (deg)	α	Gaussian	0	3

time. The following section presents a detailed study of the metamodels of the mutual inductance M, considering sources of uncertainty.

3. Metamodeling techniques introduction

This section provides an overview of the mathematical framework behind three metamodeling techniques:

- Support Vector Regression (SVR) with RBF kernel;
- Multigene Genetic Programming Algorithm (MGPA);
- Sparse Polynomial Chaos Expansions (sparse PCE).

They are considered promising techniques which allow building metamodels for the nonlinear system responses with several variables [14, 15, 20–26].

3.1. *Support vector regression metamodeling*

Support vector regression (SVR) is a metamodeling technique approximating an unknown or expensive-to-evaluate model. It represents a class of learning techniques for regression tasks developed by Vapnik [40]. This method provides significant generalization capabilities, thus making it less likely to overfit data.

SVR attempts to approximate the relationship between the input variables $x = [x_1,\ldots,x_d] \in \mathbb{R}^d$ and the output $y \in \mathbb{R}$ given a training data set of N samples $\{(\boldsymbol{x}_i, y_i)\}_{i=1}^N$ ($y = M(\boldsymbol{x})$ is the model response of the system supposed to be a scalar quantity with a finite variance, where M is a numerical model presenting the observed phenomenon). It achieves this through the equation [14, 18, 21]:

$$\mathscr{M}^{\text{SVR}}(\boldsymbol{x}) = \boldsymbol{w}^T \Phi(\boldsymbol{x}) + b \tag{2}$$

where $\Phi(\boldsymbol{x}) = [\phi_1(\boldsymbol{x}),\ldots,\phi_D(\boldsymbol{x})]$ is a nonlinear mapping function $\Phi(\cdot): \mathbb{R}^d \to \mathbb{R}^D$ which maps the parameter space of dimension d into the corresponding *feature space* of dimension D; $\boldsymbol{w} \in \mathbb{R}^D$ is
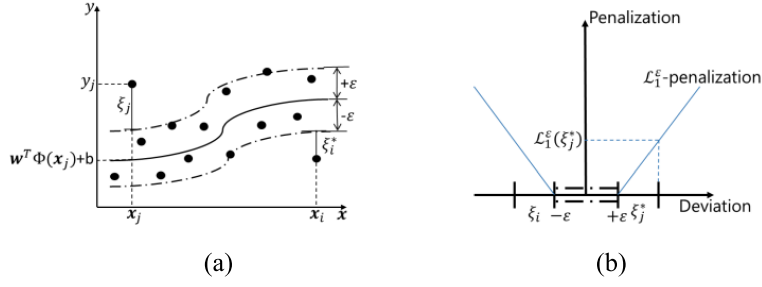
Figure 7. (a) Only the vectors outside the ε -insensitive tube (dotted line area) are penalized; (b) Penalization of deviations larger than ε for $\mathscr{L}^\varepsilon$ loss function [14, 15, 18].

a vector collecting the unknown coefficients of the nonlinear regression; $b \in \mathbb{R}$ is a bias term that is retrieved as a by-product of the solution in [14, 15, 18]; $\boldsymbol{w}^T \Phi(\boldsymbol{x})$ is defined as the inner product in $\mathbb{R}^D$ [18]. The dimensionality of the *feature space D* is defined by the nonlinear map $\Phi(\boldsymbol{x})$.

Assuming that we can tolerate a deviation of at most ε between $\mathscr{M}^{\text{SVR}}(\boldsymbol{x})$ and y, so only when the absolute value of the difference between $\mathscr{M}^{\text{SVR}}(\boldsymbol{x})$ and y is greater than ε, it needs to reduce this deviation. Then, the SVR model expression can be formalized to find $\boldsymbol{w}$ following the minimization equation [18]:

$$\min_{\boldsymbol{w}} \frac{1}{2} \|\boldsymbol{w}\|^2 + C \sum_{i=1}^{N} \mathscr{L}^\varepsilon(\mathscr{M}^{\text{SVR}}(\boldsymbol{x}_i), y_i) \tag{3}$$

where $C \in \mathbb{R}^+$ is a regularization parameter, chosen by cross-validation, which provides a trade-off between the accuracy of the model on the training data set and its flatness to avoid overfitting leading to an oscillating behavior [18]; $\mathscr{L}^\varepsilon$ is the ε-insensitive loss function, which is most widely used as follows (called: $\mathscr{L}_1$-penalization) [14, 15, 18]:

$$\mathscr{L}_1^\varepsilon(\boldsymbol{x}; y) = \begin{cases} 0 & \text{if } |\mathscr{M}^{\text{SVR}}(\boldsymbol{x}) - y| < \varepsilon, \\ (|\mathscr{M}^{\text{SVR}}(\boldsymbol{x}) - y| - \varepsilon) & \text{otherwise.} \end{cases} \tag{4}$$

A nonlinear regressor considering this loss function is illustrated in Figure 7(a). Any point that is outside the ε-insensitive tube needs to be penalized, illustrated in Figure 7(b). The best combination of the parameters $(\boldsymbol{w}, b)$ minimizes the deviation of the model predictions from the training samples outside the ε-intensive zone.

The parameters for building an SVR metamodel in this chapter are shown below, implemented within UQLAB version 2.0 [18, 41], which is fully compatible with the MATLAB environment. UQLAB is a general purpose Uncertainty Quantification framework developed at ETH Zurich (Switzerland), which is made of open-source scientific modules.

- Loss function: L_1 ε-insensitive.
- Kernel function: Gaussian radial basis function (RBF)

$$k_{\text{Gaussian}}(\boldsymbol{x}_i, \boldsymbol{x}_j) = \exp\left(-\frac{\|\boldsymbol{x}_i - \boldsymbol{x}_j\|^2}{2\sigma^2}\right) \tag{5}$$

where $\|\boldsymbol{x}_i - \boldsymbol{x}_j\|$ is the Euclidean distance between $\boldsymbol{x}_i$ and $\boldsymbol{x}_j$. The larger this distance, the smaller the value of RBF. $\sigma > 0$ is the width of the RBF. The smoothness of the Gaussian RBF is controlled by the magnitude of σ (the higher σ, the smoother the Gaussian RBF).

3.2. *Multigene genetic programming algorithm metamodeling*

In MGPA, each prediction M^{MGPA} of the model output is formed by the weighted output of the genes plus a bias term. Each gene is a function of the d input variables $\boldsymbol{x} = \{x_1, \ldots, x_d\}$ of the system. Given a training data set of N samples $\{(\boldsymbol{x}_i, y_i)\}_{i=1}^{N}$ ($y = M(\boldsymbol{x})$ is the model response of the system supposed to be a scalar quantity with a finite variance, where M is a numerical model presenting the observed phenomenon), the MGPA metamodel can be expressed as [19]:

$$M^{\text{MGPA}}(\boldsymbol{x}) = d_0 + d_1 \times \text{gene } 1 + \cdots + d_Q \times \text{gene } Q$$

$$= d_0 + d_1 \times \boxed{} + d_2 \times \boxed{} + \cdots + d_Q \times \boxed{} \tag{6}$$

where d_0 is the bias term, $d_1, \ldots, d_Q$ are the gene weights and Q is the number of genes. The weights $\boldsymbol{d}(\boldsymbol{d} = [d_0 \, d_1 \cdots d_Q])$ for the genes are automatically determined by using an ordinary least square method to regress the genes against a training data set [19]. Each gene combines a set of elementary functions with the input variables (such as sum, multiplication, division, logarithm, arctangent, hyperbolic tangent, sine, exponential, power function, etc.), and the gene depth is the number of levels in the gene structure. The expression of the MGPA metamodel is evolved automatically by using the training data set [19, 22, 23].

The process of building a metamodel with the MGPA method is [19]:

(1) Load the training data set (a set of existing input values and corresponding model response values);

(2) The genetic algorithm works on a population of metamodels, each one representing a potential solution for expressing the relationship between the input variables and the model response. The initial population of the metamodels is evolved automatically by using the training data set. During its evolution, this algorithm transforms the current population of metamodels into a new population by applying the classical genetic operations (selections, cross over, mutation, etc.) [42]. When it achieves the maximum generation, the MGPA metamodel will be picked out in terms of high coefficient of determination (R^2) and low model complexity [19]. The model complexity is computed as the simple sum of the number of nodes (the number of elementary functions plus the number of occurrences of the input variables) inside its constituent genes [43], and R^2 is calculated as below [19]:

$$R^2 = 1 - \frac{\sum_{i=1}^{N}(M(\boldsymbol{x}_i) - M^{\text{MGPA}}(\boldsymbol{x}_i))^2}{\sum_{i=1}^{N}\left(M(\boldsymbol{x}_i) - \frac{1}{N}\sum_{i=1}^{N}M(\boldsymbol{x}_i)\right)^2} \tag{7}$$

where $M(\boldsymbol{x}_i)$ is the ith value from the studied system, $M^{\text{MGPA}}(\boldsymbol{x}_i)$ is the predicted value on the MGPA metamodel, and N is the number of samples in the training data set. This value ranges from 0 to 1.

The MGPA toolbox is provided by GPTIPS, which is a free, open-source MATLAB-based software platform [19]. It can automatically evolve both the structure and the parameters of the mathematical model from the training data set. However, how to appropriately define the maximum number of genes and the maximum gene depth for an accurate MGPA metamodel needs to be carefully considered.

3.3. *Sparse polynomial chaos expansions metamodeling*

Polynomial Chaos Expansions (PCE) is a metamodeling technique that provides a functional approximation for the relationship between the input variables and model output in a non-intrusive way [20, 44]. It means that it focuses only on the one-to-one mapping relationship between input and output. Furthermore, the post-process of the PCE metamodel can also help to find the most influential input variable to the model output.

It starts by considering the vector $\boldsymbol{x} \in \mathbb{R}^d$ collecting d independent input variables $\{x_1, \ldots, x_d\}$ with a joint probability density function (PDF) $f_X(x)$, representing the input variables of the physic system. Given a training data set of N samples $\{(\boldsymbol{x}_i, y_i)\}_{i=1}^N$ ($y = M(\boldsymbol{x})$ is the model response of the system supposed to be a scalar quantity with a finite variance, where M is a numerical model presenting the observed phenomenon), the PCE metamodel is established to simulate the varying trend of the model response [20, 44]:

$$M^{\mathrm{PCE}}(\boldsymbol{x}) = \sum_{\alpha \in \mathbb{N}^d} \hat{c}_\alpha \Phi_\alpha(\boldsymbol{x}) \tag{8}$$

where $\hat{c}_\alpha$ are the unknown deterministic coefficients, and $\Phi_\alpha(\boldsymbol{x})$ are multivariate polynomials basis functions which are orthonormal with respect to the joint PDF $f_x(x)$. $\alpha \in \mathbb{N}^d$ is a multi-index that identifies the components of the multivariate polynomials Φ_α. If the input variables have a uniform distribution, the orthogonal polynomial is Legendre; while if the input variables have a Gaussian distribution, the orthogonal polynomial is Hermite [44].

The coefficients $\hat{c}_\alpha$ are obtained by post-processing the experimental design $\{(\boldsymbol{x}_i, y_i)\}_{i=1}^N$, a training data set consisting of N samples of the input variables and the corresponding model responses y. From the set of model responses, the coefficients can be estimated by the ordinary least square regression method [16, 20, 44]. For this, the infinite series in Equation (9) has to be truncated. Choosing a maximum polynomial degree p, the usual truncation scheme preserves all polynomials associated with the set [16, 20, 44]:

$$\mathscr{A}^{d,p} = \left\{ \alpha \in \mathbb{N}^d : \|\alpha\|_1 = \sum_{i=1}^d \alpha_i \le p \right\}. \tag{9}$$

Thus, the cardinal of the set $\mathscr{A}^{d,p}$ denoted $L = (d+p)!/d!p!$ increases quickly with the number of input variables d and the degree p of the polynomials [16, 20]. This leads that the size of the PCE retained in the set $\mathscr{A}^{d,p}$ will be too large when dealing with high-dimensional problems.

In order to overcome this limitation, a hyperbolic truncation strategy $\mathscr{A}_q^{d,p}$ based on the total degree p and a parameter q, with $0 < q < 1$, allowing for reduction of the size of the PCE basis is then defined as follows [16, 20, 44]:

$$\mathscr{A}_q^{d,p} = \left\{ \alpha \in \mathbb{N}^d : \|\alpha\|_q = \left(\sum_{i=1}^d \alpha_i^q \right)^{1/q} \le p \right\}. \tag{10}$$

This favors the most relevant effects and low-order interactions, which are known to have the largest impact on the variability of the model response according to the sparsity-of-effects principle [44]. It is important to point out that lower values of q imply a larger number of neglected high-rank interactions. In addition, when $q = 1$, this scheme is equivalent to the standard PCE. When $q < 1$, the retained terms of the polynomial basis can be substantially reduced [20, 44].

3.4. *Error estimates of a metamodel*

After the metamodel is constructed, its accuracy can be quantified by estimating the Root Mean Square Error (RMSE) obtained with the metamodel on the training data set. It is defined as:

$$\varepsilon_{\mathrm{RMSE}} = \sqrt{\frac{\sum_{i=1}^{\mathrm{N}}(M^{\mathrm{metamodel}}(\boldsymbol{x}_i) - M(\boldsymbol{x}_i))^2}{N}} \tag{11}$$

where $M(\boldsymbol{x}_i)$ is the model response of the training data set, $M^{\mathrm{metamodel}}(\boldsymbol{x}_i)$ is the prediction value from the metamodels above, and N is the number of samples in the training data set.

Except for the training data set used to construct the metamodel, a test data set different from the training samples, can be used to validate the predictive performance. The test error between the test data set and the predictive values on the metamodel can also be calculated by RMSE.

4. Metamodeling techniques for square couplers taking into account sources of uncertainty

Here, the SVR with RBF kernel, MGPA, and the sparse PCE metamodeling techniques are implemented to build a metamodel for small-scale square couplers and are compared below. The results given in this section were done with a XEON E5-1620, 8-core processor, working at 3.70 GHz. The 3D model of the couplers is obtained by COMSOL 5.6, and the SVR and PCE metamodels are calculated in MATLAB 2019b with the UQLAB Framework, while the MGPA metamodel is calculated in MATLAB 2017b due to the limitation of the GPTIPS toolbox functions.

The SVR with RBF kernel, MGPA, and the sparse PCE methods have been adopted to quantify the impact of these uncertainty parameters on the mutual inductance M of small-scale square couplers. In addition, the parameters on MGPA and sparse PCE methods are chosen considering the metamodel accuracy and the computational time to build an accurate metamodel. The SVR with RBF kernel builds a metamodel in light of the L_1 ε-insensitive loss function. The MGPA metamodel is performed with the following settings: Population size = 300, Number of generations = 100, Maximum number of genes = 6, and Maximum gene depth = 4. The sparse PCE metamodel is constructed by the adaptive degree method [20, 44], in which the degree of PCE metamodel varies from 3 to 15 to select the most accurate one. The hyperbolic scheme in Equation (10) is set to $q = 0.75$ to reduce the size of the polynomial basis.

1000 samples are chosen by the Latin hypercube sampling (LHS) method [45] and formed as the database. All metamodels have been trained from the same training dataset containing around one-third of the samples of the database. This data set results from COMSOL simulations with a computational cost of 6 h (one simulation with the full solver takes about 50 s). To investigate the performance of the obtained metamodels, their predictions are then compared with a test data set containing the remaining database samples. Table 4 provides a detailed comparison of the accuracy and the computational cost of the proposed metamodeling techniques by collecting the RMSE on the training data set and the test data set, along with the corresponding computational time t_{training} and the predictive time $t_{\mathrm{predictive}}$ (to predict one output) respectively. It also shows that the sparse PCE metamodel turns out to use the least computational time and to be the most accurate metamodel with a training RMSE and a test RMSE, which is better than the accuracies obtained by the SVR and MPGA metamodels.

Furthermore, another 1000 samples selected by the MC method are computed in COMSOL to form a new data set. Figure 8 provides the scatter plots for the metamodels of the mutual inductance on the SVR, MGPA, and sparse PCE methods. These plots emphasize a good agreement between these metamodels and this data set because the samples are very close to the solid lines.

(a)

(b)

(c)
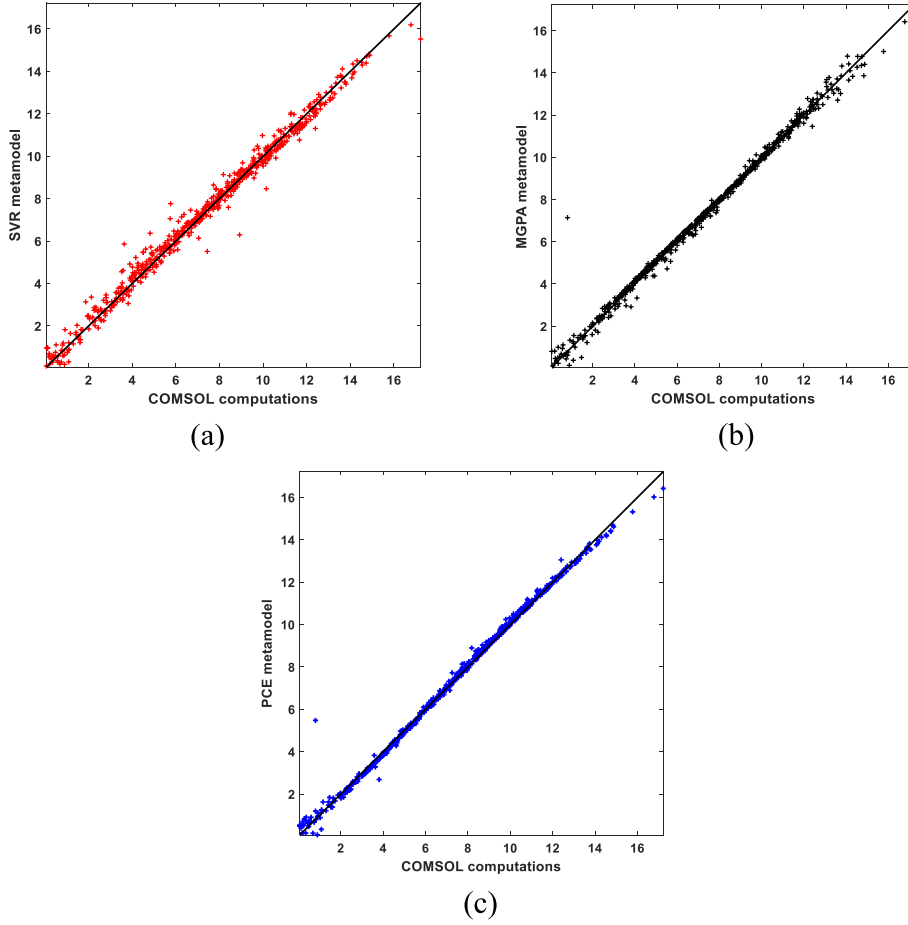
Figure 8. Scatter plots of the mutual inductance providing a comparison among the predictions of the SVR metamodel with RBF kernel (red marker in (a)), the MGPA metamodel (black marker in (b)), the sparse PCE metamodel (blue marker in (c)) and the results of COMSOL computations.

Table 4. Comparison of the accuracy and the computational cost of the SVM, MPGA, and PCE metamodels computed for the square couplers

Method	Training RMSE	Test RMSE	t_{training}	$t_{\text{predictive}}$
COMSOL computations	-	-	6.45 h	60 s
SVR (RBF)	0.0266	0.0420	2.48 s	<1 s
MGPA	0.0233	0.0475	313.54 s	<1 s
Sparse PCE	0.0158	0.0270	0.357 s	<1 s

Then, the impact of the influencing factors on the mutual inductance is illustrated in Figure 9, where the probability density functions (PDFs) of the mutual inductance estimated via the SVR, MGPA, and sparse PCE metamodels are compared with the PDF of the COMSOL computations. It can be seen that the variability of the mutual inductance is well captured by these metamodels, which confirms a good estimation of the PDF of the mutual inductance with these metamodels and highlights a similar level of accuracy. In terms of computational cost, this data set, including
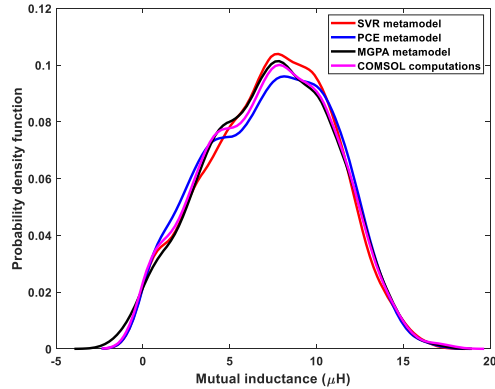
Figure 9. PDFs of the mutual inductance obtained from the SVR (solid red curve), MGPA (solid black curve) and sparse PCE metamodels (solid blue curve) compared with the PDF of COMSOL computations (solid magenta curve).

1000 samples, required about 14 h to compute in COMSOL, while the metamodels on the SVR, MGPA, and sparse PCE need less than 1 minute. It is worth noting that this computational cost does not include the time to generate the training samples from LHS in COMSOL, which were needed for constructing the metamodels.

Compared to the other metamodeling techniques based on the same dataset, the sparse PCE metamodeling technique uses less time to build a metamodel and provides more accurate results. So, it is meaningful to choose such an approach to analyse the performances of the coupler, taking into account the sources of uncertainty.

5. Conclusion

This paper provides an overview of SVR with RBF kernel, MGPA, and PCE metamodeling techniques and their application in case of analyzing an IPT system. When the metamodels are built by these techniques, the ways to evaluate the accuracy and build the PDF are also summarized. Some metamodeling techniques (SVR with RBF kernel, MGPA, and sparse PCE) are built and compared for analyzing the mutual inductance *M* of the magnetic couplers considering sources of uncertainty. Due to the tradeoff between the computational time and the accuracy of the metamodel, the sparse PCE metamodeling technique appears to be a very useful tool in the analysis of IPT systems. Then, it will be used in the next step to address the magnetic and thermal coupled field analysis. Indeed, when a high-power IPT system works for a long time, the heating of the magnetic coupler brings adverse effects on the efficiency and stability of the system. An accurate prediction of such a phenomenon will improve the assessment of IPT performances.

Declaration of interests

The authors do not work for, advise, own shares in, or receive funds from any organization that could benefit from this article, and have declared no affiliations other than their research organizations.

References

[1] M. Eshani *et al.*, "Modern electric, hybrid electric and fuel cell vehicles", in *Fundamentals, Theory, and Design*, CRC Press, Boca Raton, FL, 2005.

[2] M. Yilmaz, P. T. Krein, "Review of battery charger topologies, charging power levels, and infrastructure for plug-in electric and hybrid vehicles", *IEEE Trans. Power Electron.* **28** (2013), no. 5, p. 2151-2169.

[3] C. T. Rim, C. Mi, "Wireless Power Transfer for Electric Vehicles and Mobile Devices | IEEE eBooks | IEEE Xplore", Accessed: July 10, 2024. [Online]. Available: https://ieeexplore.ieee.org/book/7953908.

[4] T. M. Fisher *et al.*, "Electric vehicle wireless charging technology: a state-of-the-art review of magnetic coupling systems", *Wireless Power Transf.* **1** (2014), no. 2, p. 87-96.

[5] "J1772_202401 : SAE Electric Vehicle and Plug-in Hybrid Electric Vehicle, Conductive Charge Coupler - SAE International", Accessed: July 10, 2024. [Online]. Available: https://www.sae.org/standards/content/j1772_202401/.

[6] "Charger Types and Speeds | US Department of Transportation", Accessed: July 10, 2024. [Online]. Available: https://www.transportation.gov/rural/ev/toolkit/ev-basics/charging-speeds.

[7] Z. J. Lee, J. Z. Pang, S. H. Low, "Pricing EV charging service with demand charge", *Electr. Power Syst. Res.* **189** (2020), article no. 106694.

[8] A. Mahesh, B. Chokkalingam, L. Mihet-Popa, "Inductive wireless power transfer charging for electric vehicles—a review", *IEEE Access* **9** (2021), p. 137667-137713, https://10.1109/ACCESS.2021.3116678.

[9] C. Panchal, S. Stegen, J. Lu, "Review of static and dynamic wireless electric vehicle charging system", *Eng. Sci. Technol. Int. J.* **21** (2018), no. 5, p. 922-937, https://10.1016/j.jestch.2018.06.015.

[10] "Electric Vehicles - Worldwide – Statista Market Forecast", Statista. Accessed: July 10, 2024. [Online]. Available: https://www.statista.com/outlook/mmo/electric-vehicles/worldwide.

[11] M. Larbi *et al.*, "Variability impact of many design parameters: the case of a realistic electronic link", *IEEE Trans. Electromagn. Compat.* **60** (2018), no. 1, p. 34-41.

[12] S. De Ridder *et al.*, "A generative modeling framework for statistical link analysis based on sparse data", *IEEE Trans. Compon. Packag. Manuf. Technol.* **8** (2018), no. 1, p. 21-31.

[13] V. Cirimele *et al.*, "Uncertainty quantification for SAE J2954 compliant static wireless charge components", *IEEE Access* **8** (2020), p. 171489-171501.

[14] R. Trinchero *et al.*, "Machine learning and uncertainty quantification for surrogate models of integrated devices with a large number of parameters", *IEEE Access* **7** (2019), p. 4056-4066.

[15] R. Trinchero *et al.*, "Machine learning for the performance assessment of high-speed links", *IEEE Trans. Electromagn. Compat.* **60** (2018), no. 6, p. 1627-1634.

[16] B. Sudret, "Global sensitivity analysis using polynomial chaos expansions", *Rel. Eng. Syst. Saf.* **93** (2008), no. 7, p. 964-979.

[17] I. M. Sobol, "Sensitivity estimates for nonlinear mathematical models", *Math. Model. Comput. Exp.* **1** (1990), no. 4, p. 407-414.

[18] M. Moustapha *et al.*, "UQLab user manual – Support vector machines for regression", in *Report UQLab-V2.0-111, Chair of Risk, Safety and Uncertainty Quantification*, ETH Zurich, Switzerland, 2022.

[19] D. P. Searson, "GPTIPS 2: an open-source software platform for symbolic data mining", in *Handbook of Genetic Programming Applications* (A. H. Gandomi, A. H. Alavi, C. Ryan, eds.), Springer International Publishing, Cham, 2015, p. 551-573.

[20] G. Blatman, B. Sudret, "Adaptive sparse polynomial chaos expansion based on least angle regression", *J. Comput. Phys.* **230** (2011), no. 6, p. 2345-2367.

[21] J. A. K. Suykens *et al.*, *Least Squares Support Vector Machines*, World Scientific, Singapore, 2002.

[22] G. D. Capua *et al.*, "Mutual inductance behavioral modeling for wireless power transfer system coils", *IEEE Trans. Ind. Electron.* **68** (2021), no. 3, p. 2196-2206.

[23] A. Delgado *et al.*, "Self and mutual inductance behavioral modeling of square-shaped IPT coils with air gap and ferrite core plates", *IEEE Access* **10** (2022), p. 7476-7488.

[24] G. Di Capua *et al.*, "Analysis of dynamic wireless power transfer systems based on behavioral modeling of mutual inductance", *Sustainability* **13** (2021), no. 5, article no. 2556.

[25] Y. Pei *et al.*, "Comparison of coupling coils for static inductive power-transfer systems taking into account sources of uncertainty", *Sustainability* **13** (2021), no. 11, article no. 6324.

[26] Y. Pei *et al.*, "Fast shielding optimization of an inductive power transfer system for electric vehicles", *IEEE Access* **10** (2022), p. 91227-91234.

[27] A. Triviõ-Cabrera, J. M. González-González *et al.*, "Wireless Power Transfer for Electric Vehicles: Foundations and Design Approach", Accessed: July 10, 2024. [Online]. Available: https://link.springer.com/book/10.1007/978-3-030-26706-3.

[28] "Vehicle Initiative Consortium for Transport Operation and Road Inductive Applications", Victoria Project, April 25, 2017. http://greentechlatvia.eu/wp-content/uploads/bsk-pdf-manager/1-8_Project_Victoria_(Bludszuweit)_8.pdf (accessed September 19, 2022).

[29] V. Cirimele, M. Diana, F. Freschi, M. Mitolo, "Inductive power transfer for automotive applications: state-of-the-art and future trends", *IEEE Trans. Indus. Appl.* **54** (2018), no. 5, p. 4069-4079.

[30] G. A. Covic, J. T. Boys, "Modern trends in inductive power transfer for transportation applications", *IEEE J. Emerging Sel. Top.n Power Electron.* **1** (2013), no. 1, p. 28-41.

[31] M. Ibrahim, *Wireless Inductive Charging for Electrical Vehicles: Electromagnetic Modelling and Interoperability Analysis*, Phd thesis, 2014, Université Paris Sud – Paris XI. Accessed February 11, 2024. [Online]. Available: https://tel.archives-ouvertes.fr/tel-01127163.

[32] P. S. R. Nayak, D. Kishan, "Design and analysis of SS resonant IPT system with computed mutual inductance through FEM model", in *2018 International Conference on Power, Instrumentation, Control and Computing (PICC), Thrissur, India, January*, 2018, p. 1-5.

[33] K. Kadem *et al.*, "Optimal coupler topology for dynamic wireless power transfer for electric vehicle", *Energies* **14** (2021), no. 13, article no. 3983.

[34] K. Kadem, *Modélisation et optimisation d'un coupleur magnétique pour la recharge par induction dynamique des véhicules électriques*, Theses, Centralesupelec, 2020, Accessed August 29, 2022. [Online]. Available: https://hal.archives-ouvertes.fr/tel-03253967.

[35] R. Bosshard, J. Mühlethaler, J. W. Kolar, I. Stevanović, "Optimized magnetic design for inductive power transfer coils", in *2013 Twenty-Eighth Annual IEEE Applied Power Electronics Conference and Exposition (APEC), Long Beach, CA, USA, March*, 2013, p. 1812-1819.

[36] R. Bosshard, J. W. Kolar, J. Mühlethaler, I. Stevanović, B. Wunsch, F. Canales, "Modeling and η - α -pareto optimization of inductive power transfer coils for electric vehicles", *IEEE J. Emerging Sel. Top. Power Electron.* **3** (2015), no. 1, p. 50-64.

[37] R. W. Erickson, D. Maksimović, "Inductor design", in *Fundamentals of Power Electronics* (R. W. Erickson, D. Maksimović, eds.), Springer US, Boston, MA, 2001, p. 539-564.

[38] "J2954 : wireless power transfer for light-duty plug-in/electric vehicles and alignment methodology - SAE International", Accessed: July 10, 2024. [Online]. https://www.sae.org/standards/content/j2954_202010/.

[39] "Software for Simulating Static and Low-Frequency Electromagnetics", COMSOL. Accessed: July 10, 2024. https://www.comsol.com/acdc-module.

[40] V. N. Vapnik, *The Nature of Statistical Learning Theory*, Springer, New York, NY, 2000, Accessed: July 10, 2024. [Online]. Available: https://link-springer-com.ezproxy.universite-paris-saclay.fr/book/10.1007/978-1-4757-3264-1.

[41] S. Marelli, B. Sudret, "UQLab: a framework for uncertainty quantification in Matlab", in *Proceedings of the 2nd International Conference on Vulnerability, Risk Analysis and Management (ICVRAM2014), Liverpool, United Kingdom*, 2014, p. 2554-2563.

[42] M. Mitchell, *An Introduction to Genetic Algorithms*, The MIT Press, Cambridge, MA, 1998, Accessed: July 10, 2024. [Online]. Available: https://mitpress.mit.edu/books/introduction-genetic-algorithms.

[43] G. F. Smits, M. Kotanchek, "Pareto-front exploitation in symbolic regression", in *Genetic Programming Theory and Practice II* (U.-M. O'Reilly, T. Yu, R. Riolo, B. Worzel, eds.), Springer US, Boston, MA, 2005, p. 283-299.

[44] S. Marelli, N. Luthen, B. Sudret, *UQLab user manual – Polynomial chaos expansions, Report UQLab-V2.0-104, Chair of Risk, Safety and Uncertainty Quantification*, ETH Zurich, Switzerland, 2022.

[45] C. Lataniotis *et al.*, *UQLab user manual – The Input module, Report UQLab-V2.0-102, Chair of Risk, Safety and Uncertainty Quantification*, ETH Zurich, Switzerland, 2022.